AIMS Materials Science, 12(2): 363–379.
DOI: 10.3934/matersci.2025019
Received: 20 February 2025
Revised: 19 May 2025
Accepted: 28 May 2025
Published: 04 June 2025

http://www.aimspress.com/journal/Materials

Research article

Effect of raster angle on the tensile and flexural strength of 3D printed PLA+ parts

Juan Sebastián Ramírez-Prieto, Juan Sebastián Martínez-Yáñez and Andrés Giovanni González-Hernández*

Grupo de Investigación en Desarrollo y Tecnología de Nuevos Materiales (GIMAT), Universidad Industrial de Santander, Carrera 27 calle 9, Bucaramanga, Santander, 680006, Colombia

* **Correspondence:** Email: aggonzal@uis.edu.co; Tel: +57-607-634-4000.

Abstract: In fused deposition modeling (FDM) 3D printing, the properties and performance of the fabricated components are profoundly affected by the selected process parameters. Therefore, it is crucial to choose and optimize these parameters to improve the quality and mechanical characteristics of the final product. Given this, the present study explored the mechanical properties of 3D-printed components fabricated from polylactic acid (PLA)+ filament, specifically examining how different raster angles influence their flexural and tensile performance. Three raster angle conditions were investigated: parallel (0°/0°), grid (0°/90°), and crisscross (45°/–45°). The results demonstrate that the raster angle has a significant effect on the flexural and tensile strength of the printed specimens. The parallel raster (0°/0°) produced the highest flexural strength, attributed to the alignment of the fibers perpendicular to the applied load, which enhances the load capacity. Conversely, the crisscross (45°/–45°) orientation resulted in the lowest flexural strength but exhibited greater ductility, as evidenced by extensive plastic deformation. This increased ductility is attributed to the material's ability to absorb more energy before failure, resulting from favorable shear deformation dynamics. In tensile testing, the parallel raster (0°/0°) showed superior strength, while the grid and crisscross orientations followed with progressively lower values. The fracture behavior revealed that samples 3D printed with a 45°/–45° raster angle tend to fail along the raster orientation, primarily due to the development of shear stresses.

Keywords: additive manufacturing; FDM; raster angle; filling direction; tensile strength; PLA+

1. Introduction

Additive manufacturing (AM) has presented various new opportunities in product design and engineering [1]. AM methods offer parts based on faster and more flexible procedures than conventional manufacturing processes [2,3]. Consequently, this technology enables the production of a prototype from a 3D model, proving valuable in both the design phase and in preparation for manufacturing [4]. 3D-printed parts are currently employed as prototypes and final products [5].

Furthermore, 3D printing presents several competitive advantages over conventional manufacturing methods, including reduced cost, simplified fabrication, shortened time between design and final part acquisition, minimized waste generation, and incorporation as an Industry 5.0 technology [2]. On the other hand, it is noteworthy that a wide range of industries, including automotive, aerospace, medical, mechanical, food, fashion, architecture, chemical, construction, electrical, electronics, and education, among others, are capitalizing on the benefits of 3D printing [6].

Among the different AM methods, fused deposition modeling (FDM) is the most prevalent technology due to its user-friendliness, economic feasibility, and widespread commercial availability of feedstock materials [6]. FDM is a technique that involves extruding a filament through a heated nozzle. The filament melts and reaches the nozzle in a semi-liquid state. The printing process operates by displacing the nozzle along the XY plane, enabling the precise formation of two-dimensional cross-sectional geometries. Concurrently, the build platform (or bed) undergoes incremental vertical displacement along the Z-axis. This coordinated motion facilitates the sequential deposition of material layers, thereby constructing the final three-dimensional structure. The controlled movement of the nozzle in the XY plane defines the in-plane geometry. At the same time, the layer-wise advancement of the platform in the Z direction results in the additive formation of the volumetric object [2].

A diverse range of thermoplastics are employed in FDM 3D printing, with the most prevalent being polylactic acid (PLA) [3], acrylonitrile butadiene styrene (ABS), polycarbonates (PC), polyetherether ketone (PEEK), nylon (N), polyetherimide (PEI), and polycaprolactone (PCL) [7,8]. Among these, PLA is one of the most favorable polymers for FDM 3D printing due to its low melting temperature, biodegradability, and printability [9–11]. PLA has garnered significant attention from researchers due to its heightened sensitivity to process parameters compared to ABS [2,12]. Numerous FDM printing parameters have been extensively researched, including layer geometry patterns, nozzle and bed temperatures, layer thickness, infill percentages, printing speeds, number of part contours, build times, moisture contents, and others [13–16]. However, based on these studies, it has been established that the parameters that most significantly influence the properties of parts produced using 3D printing technology are layer height, infill pattern and geometry, build orientation, and infill density [17–20].

The influence of FDM printing parameters on the mechanical properties of 3D printed parts has been extensively studied, focusing on tensile behavior [21–24]. Researchers have demonstrated that increasing infill density enhances tensile strength [25–28]. For instance, Khan [20] found that the infill pattern plays a crucial role in determining the mechanical properties of 3D-printed PLA parts. The rectilinear pattern exhibited the highest performance at a constant infill density of 20%, achieving a tensile strength of 19.1 MPa and an elastic modulus of 10.51 GPa. In flexural testing, this pattern reached a maximum flexural strength of 24.4 MPa and a tangent modulus of 0.359 GPa, clearly outperforming the concentric, honeycomb, and Hilbert curve patterns [20]. In another work, Kadhum et al. [29] demonstrated that the selection of infill pattern plays a crucial role in dictating both

the mechanical performance and surface quality of 3D-printed parts made from PLA, PLA+, and PETG materials. Their extensive study, which employed a constant 20% infill density across fourteen distinct patterns, revealed that the optimal tensile strengths were achieved using the cubic, gyroid, and concentric patterns for PLA, PETG, and PLA+, respectively recording maximum ultimate tensile strengths of 15.6, 20.8, and 16.5 MPa [29]. In another work, Tan et al. [30] demonstrated that infill density and raster angle critically influence the mechanical properties of 3D-printed PLA specimens. The results revealed that a 0° raster angle combined with 100% infill density yields the highest tensile strength and Young's modulus [30]. As mentioned earlier, these works underline the need to optimize printing parameters to tailor the mechanical performance of PLA parts to specific engineering applications.

On the other hand, layer thickness exhibits a less pronounced effect on the mechanical strength of 3D printed parts. While an increase in layer thickness leads to a slight rise in tensile strength up to a certain point, the overall impact is relatively minor [31,32]. Investigations into the influence of build orientations on mechanical strength, particularly tensile strength, reveal that build orientations have a significant impact on the mechanical behavior of printed parts [27]. A detailed analysis of various process parameters shows that the angle of the raster pattern is a critical factor in determining the mechanical strength of 3D-printed parts [33–35]. For instance, Gopi et al. [27] reported that the mechanical performance of FDM-printed PLA parts is significantly influenced by raster orientation. In particular, specimens printed with a 45°/–45 ° raster pattern exhibit superior flexural and impact strengths compared to those printed with a 0°/90° orientation, while compressive strengths remain relatively similar across both configurations. This indicates that the denser and more interlocked raster arrangement in the 45°/–45° pattern enhances load distribution and energy absorption during deformation. In another work, Ayatollahi et al. [36] demonstrated that in-plane raster orientation critically governs tensile and fracture behaviors in FDM-printed PLA specimens. The study revealed that a 45°/–45° raster pattern achieves the highest elongation at break and fracture resistance, whereas a 0°/90° orientation produces significantly lower plastic deformation and fracture load in tensile tests. Supported by detailed scanning electron microscopy (SEM) analysis and finite element simulations, these results underscore the pronounced anisotropy in mechanical properties, particularly in plastic strain, and highlight the importance of optimizing raster angles to enhance the durability and performance of 3D-printed components [35]. Another investigation is that by Khosravani et al. [37], who examined the influence of acetone-based surface treatment on the tensile and fracture behavior of 3D-printed ABS specimens with raster orientations of 0°/90° and 45°/–45°. Their results showed that, after treatment, the ultimate tensile strength decreased from 31.16 to 30.01 MPa for 0°/90° specimens and from 29.76 to 28.84 MPa for 45°/–45° specimens. The study demonstrates that while surface quality improves, chemical post-processing compromises mechanical performance, with raster orientation playing a key role in this degradation [37].

A comprehensive literature review revealed that the raster angle has emerged as a crucial parameter in numerous studies [27,30,38–41], consistently demonstrating its significant effect on the tensile [42–45] and flexural properties [46,47] of 3D-printed components across diverse materials. Slicing software utilizes a standardized infill pattern, with FDM printing building layers by first constructing the outer profile and then filling the interior sections. These infill patterns come in various forms, such as honeycomb, rectilinear, crisscross, and grid [27]. Although few studies have specifically examined the effects of a 0°/0° raster pattern, this configuration has received limited attention compared to other more commonly used deposition angles. In this study, the mechanical properties—particularly tensile and flexural strength—of 3D-printed PLA+ specimens were evaluated using three

different raster orientations: 0°/0°, 0°/90° (grid), and 45°/–45° (crisscross). The latter two patterns are typically default in most slicing software due to their well-established balance between stiffness and mechanical strength. This work aims to compare the tensile and flexural performance of PLA+ samples printed with the 0°/0° orientation against those fabricated using the grid and crisscross configurations, thereby assessing the impact of raster alignment on the mechanical behavior of 3D-printed components.

2. Materials and methods

The filament material used was PLA+, which had a diameter of 1.75 mm and was purchased from eSun. It is essential to mention that PLA is a biodegradable polymer derived primarily from renewable sources such as corn starch or sugarcane. Its low cost and excellent printability have established it as a dominant material in additive manufacturing. However, PLA has particular mechanical strength and thermal resistance limitations, leading manufacturers to develop enhanced formulations known as PLA+ (also referred to as tough PLA or pro PLA). These improved formulations incorporate various additives to increase impact resistance, heat tolerance, surface finish, and interlayer adhesion, enhancing their performance for functional and engineering applications [29]. Table 1 presents the properties as specified by the manufacturer. The ultimate tensile strength (UTS) is equal to that reported by other authors [2]. Additionally, according to the manufacturer, PLA+ filament exhibits a good balance of strength, rigidity, and toughness, as well as strong impact resistance. Additionally, the filament is composed of 92%–96% polylactic acid (PLA) (CAS No. 6100-51-6) and 2%–4% calcium carbonate (CAS No. 471-34-1); the remaining components are other additives.

Table 1. 3D-printing filament properties according to the manufacturer.

Properties	Values
Density	1.23 g/cm^3
Tensile strength	60 MPa
Elongation at break	20%
Bending strength	74 MPa
Flexural modulus	1973 MPa
Heat distortion temperature	53 °C (0.45 MPa)
Melt index	5 (190 °C/2.16 kg) g/10 min
Printing speed	40–100 mm/s
Base plate temperature	45–60 °C
Printing temperature	210–230 °C

Table 2 lists the parameters selected for printing specimens. The printing parameters were selected based on recommendations from the FlashPrint software, supported by literature data and manufacturer specifications, as long as they conformed to the range established in Table 1. This approach ensured both technical consistency and practical relevance [2]. The table also highlights the three conditions employed for raster angle variations. These conditions are designated as C1, C2, and C3, as follows:

- Condition 1 (C1): This condition utilizes a raster angle of 0°/0°, representing a parallel orientation of the raster lines along the specimen's length.

• Condition 2 (C2): In this condition, the raster angle is set to 0°/90° (grid), indicating a perpendicular alignment of the raster lines with respect to each other.

• Condition 3 (C3): This condition employs a raster angle of 45°/90° or 45°/–45° (crisscross), representing a diagonal orientation of the raster lines, creating a 45° angle with both the X and Y axes.

Table 2. Main 3D printing parameters.

Parameters	Values
Extruder temperature	220 °C
Bed temperature	60 °C
Printing speed	50 mm/s
Travel speed	100 mm/s
Infill	100%
Deposition orientation	0° (in plane)
Layer thickness	0.2 mm
Fill pattern	Lineal
Start and cross angle	C1 sample: 0°/0°
	C2 sample: 0°/90° (grid)
	C3 sample: 45°/–45° or 45°/90°(crisscross)
Outer shell	1
Inner shell	3
Overlap perimeter	30%

Figure 1 comprehensively illustrates the design of the raster angles, delineating both the initial deposition orientations and the subsequent crossing angles for each experimental condition. This schematic demonstrates the filament lay-down strategy during the additive manufacturing process, providing a precise understanding of the interlayer bonding mechanisms. Moreover, these specifically chosen raster angle configurations were implemented to evaluate their impact on the tensile and flexural performance of the 3D-printed PLA+ components.

The specimens were designed using Autodesk Fusion 360 (Educational License). This CAD software was used to generate the STL (Standard Tessellation Language) file, which was imported via the FlashPrint slicer, developed by the same company that manufactures the 3D printer used in this study. A file with a .gx extension was created by the FlashPrint slicer software. This file contains the code uploaded to the 3D printer, which governs the machine's movements, temperature settings, and other printing parameters. The 3D printer used to generate the required specimens was a FlashForge Guider III (see Figure 2).

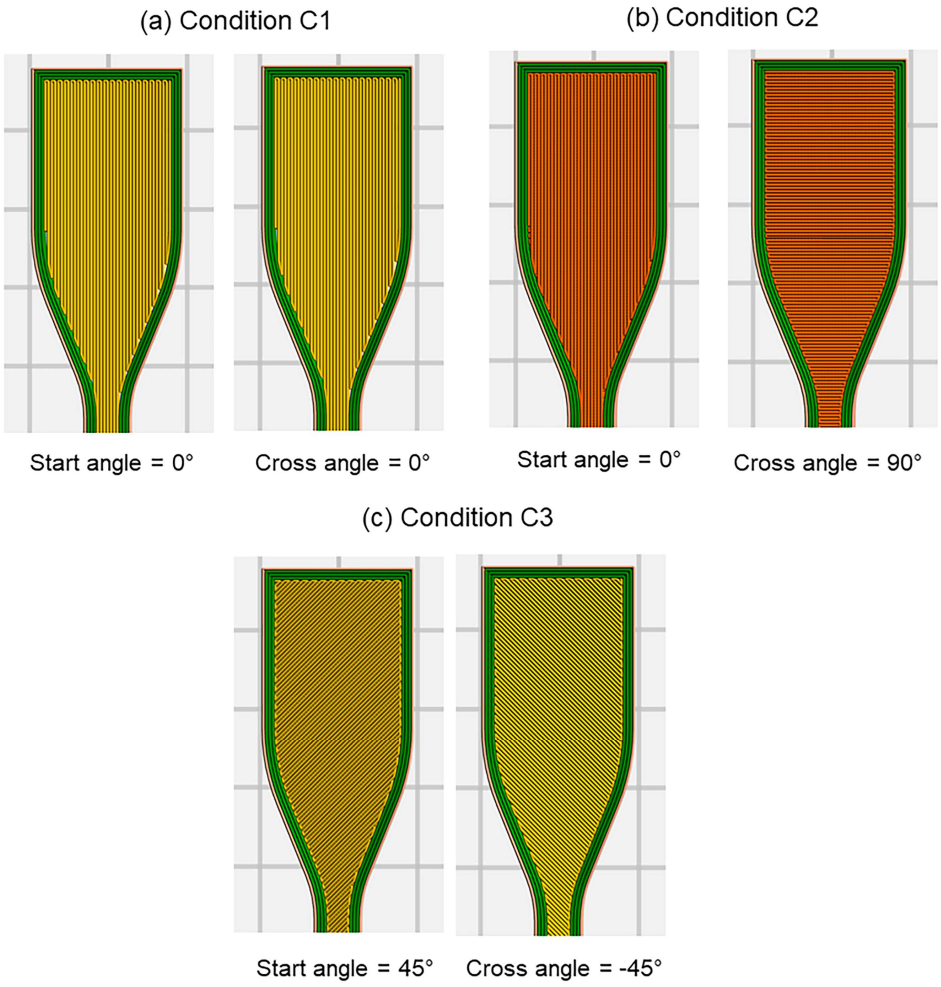

Figure 1. Pattern of the raster angles.

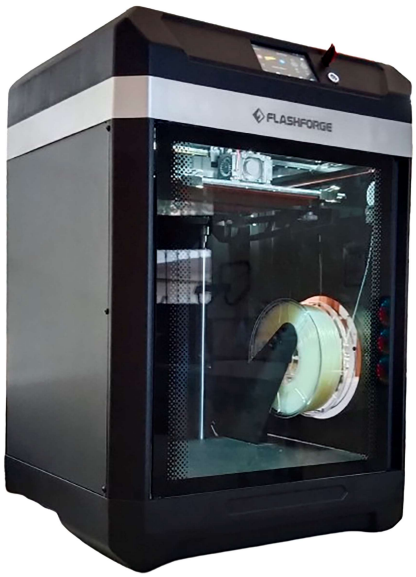

Figure 2. General view of the FlashForge Guider III 3D Printer.

The tensile and flexural tests were carried out using a Tinius Olsen universal machine, model H25KS, with a capacity of 25 kN, as shown in Figure 3. The tensile tests were carried out according to ASTM D638-22 [48] at a testing speed of 5 mm/min at room temperature. Other authors used these test conditions [2]. The flexural test was conducted according to ASTM D790-17 [49] at a speed of 2 mm/min and a span (L) of 70 mm between the two supports. When the specimen deformation reaches the specified deflection, the maximum bending stress can be referred to as the flexural strength [50]. Therefore, the flexural strength σ_f in MPa was calculated using Eq 1:

$$\sigma_f = \frac{3PL}{2bh^2} \tag{1}$$

where P is the maximum load in Newtons, b is the width of the test specimen in millimeters, and h is the depth of the test specimen in millimeters. Also, the modulus of elasticity (E_B) of the flexural tests was calculated using Eq 2. The test data were processed using OriginLab software.

$$E_B = \frac{L^2F}{4bh^3\delta} \tag{2}$$

where δ is the deflection of the sample in millimeters.

Figure 3. Universal stress machine.

The samples used for the tensile test were prepared according to ASTM D638-14 [48] using type-IV specimens. In contrast, the samples designated for the flexural tests were prepared by ASTM D790-17 [49] standards, featuring a length of 127 mm, a width of 12.7 mm, and a thickness of 3.2 mm. Each test utilized five samples, adhering to the specifications outlined in the referenced standards for this study.

3. Results and discussion

Figure 4 presents the load vs. displacement curves obtained from the flexural tests performed on the five samples for each condition of the raster angles. The graph shows that the C1 samples (0°/0°) exhibited the highest flexural strength, followed by the C2 samples (0°/90°, grid); finally, the C3 samples (45°/–45°, crisscross) displayed the lowest flexural strength. It is important to note that none of the tested samples experienced fracture, and the test was halted after verifying that the sample had reached its maximum strength. The average flexural stress and flexural modulus are shown in Table 3. The C1 samples had the highest average flexural strength of 78 MPa, while the C2 samples had an average of 52.1 MPa; finally, the C3 samples had an average of 40.7 MPa. This phenomenon can be explained by the fact that a higher number of fibers (3D-printed filament) perpendicular to the flexural load results in higher flexural strength of the component. In other words, the C1 sample, which has 100% of its fibers perpendicular to the flexural load, has the highest strength, while the C2 sample, with 50% of its fibers (grid) perpendicular to the load, has lower strength compared to the C1 sample. Finally, the behavior of fibers oriented at 45° (samples C3, crisscross) under flexural load demonstrates the lowest strength among all tested conditions. This is attributed to the tendency of these fibers to deform by shear under load, resulting in an unfavorable redistribution of stress and thereby compromising the material's overall flexural strength Therefore, it can be seen that the orientation of the raster angle influences the flexural strength, achieving greater strength when a higher number of fibers are perpendicular to the applied load. On the other hand, the elastic modulus of the samples follows the same trend, with the C1 samples having the highest modulus, followed by the C2 samples, and finally the C3 samples (see Table 3). Notably, despite their low flexural strength, C3 samples exhibited a wider range of plastic deformation in the load-displacement curves (see Figure 4, green curve), greater than that of the other samples. This indicates that the C3 samples have high ductility, meaning the material can absorb significant energy through deformation before failure. In these samples, the junction points of the fibers and layers may exhibit elastoplastic behavior, thereby reducing their flexural strength. However, these junctions between the fibers, layers, and their inherent strength allow for greater ductility of the component, avoiding a rapid decrease in the curve in the plastic zone as observed in samples C1 and C2 (see Figure 4). Comparing the results of this study with those reported by Jaya Christiyan et al. [51], a clear correlation is observed, as they demonstrated that 3D printing parameters significantly affect the flexural strength of PLA components fabricated by FDM. The highest flexural strength, 68 MPa (lower than the C1 sample), was achieved under 0° raster orientation, 0.2 mm layer thickness, and a printing speed of 38 mm/s. This enhanced performance is attributed to the increased number of layers and improved interlayer adhesion. In contrast, vertically printed specimens (90° orientation) exhibited a marked decrease in flexural strength, with values of 48 MPa for 0.2 mm, 42 MPa for 0.25 mm, and 36 MPa for 0.3 mm, all printed at a speed of 52 mm/s. Rivera-López et al. [52] reported higher flexural strength values, demonstrating that the flexural performance of FDM-printed PLA specimens is susceptible to nozzle temperature. Their experiments, conducted under controlled conditions (0.4 mm nozzle diameter, 0.2 mm layer height, and 100% infill), showed a progressive increase in flexural strength as the nozzle temperature ranged from 180 to 260 °C. The maximum flexural strength, 92.8 MPa, was achieved at 260 °C, while lower temperatures resulted in reduced values—80.2 MPa at 180 °C and 83.8 MPa at 200 °C [52].

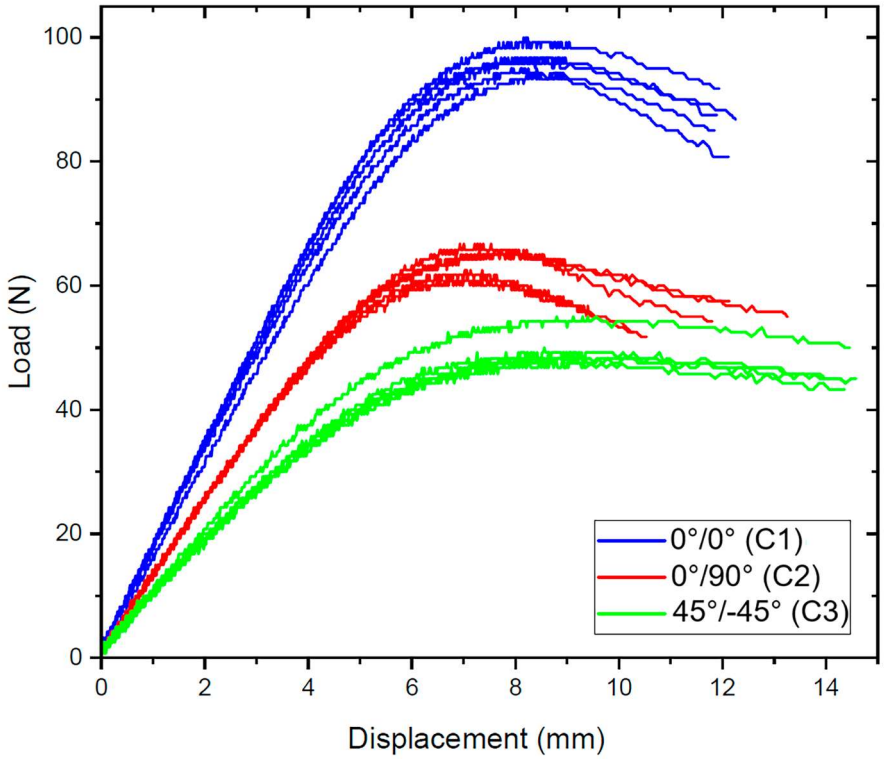

Figure 4. Load and displacement curve of flexural test for different raster angles.

Table 3. Results of the flexural test.

Sample	Flexural strength (MPa)	Modulus of elasticity (MPa)
C1	78.0 ± 1	2491 ± 67.8
C2	52.1 ± 1.3	1844 ± 50
C3	40.7 ± 1.3	1206 ± 34

The stress vs. strain curves of the C1, C2, and C3 samples obtained from tensile tests are shown in Figure 5. Most of the tested samples exhibited brittle behavior, characterized by a minimal or nonexistent plastic zone in the curve. Sample C1 demonstrated the highest tensile strength with an average ultimate tensile strength (UTS) of 38.2 MPa (see Figure 5a), followed by sample C2 with a value of 35.8 MPa (see Figure 5b). Sample C3 exhibited the lowest tensile strength with 31.5 MPa (see Figure 5c). Notably, all samples fractured, predominantly at the section change of the specimen, as observed in the bottom right part of Figure 5a–c. For comparison, other researchers have reported similar tensile strength values for PLA samples fabricated via FDM. Balasubramanian et al. [23] found that using a ±45° raster orientation, 75% infill density, and a layer thickness of 0.16 mm resulted in a tensile strength of PLA ranging from 30.91 to 38.89 MPa, depending on the applied strain rate. The maximum 38.89 MPa was recorded at an 8 mm/min cross-head speed. Tan et al. [37] reported lower tensile strength values and examined the effect of infill density and raster angle on the mechanical properties of PLA parts manufactured via FDM. Their results showed that the lowest ultimate tensile strength, 17.33 MPa, was obtained using a 30% infill density and 90° raster angle. These conditions promote weak interlayer bonding and poor stress distribution due to the filaments' orientation perpendicular to the load. In contrast, the highest strength achieved in their study was 28.93 MPa,

corresponding to 100% infill and 0° raster angle, where the filament paths are aligned with the applied force. These findings highlight that lower infill densities and unfavorable raster orientations significantly reduce the tensile performance of 3D-printed PLA, primarily due to increased porosity and reduced load transfer efficiency between layers. Other higher tensile strength values were reported by Saravana Kumar et al. [16], who investigated PLA components fabricated via material extrusion using a multi-criteria optimization approach. Using a Taguchi method, the authors identified the optimal combination of 0.1 mm layer thickness, 60 mm/s printing speed, and 200 °C printing temperature, under which the maximum ultimate tensile strength reached 45.22 MPa. This notable increase was attributed to enhanced interlayer bonding and reduced porosity, as confirmed by SEM analysis. Sandanamsamy et al. [40] reported lower tensile strength values and evaluated the influence of raster angle and printing temperature on the tensile behavior of PLA parts produced via FDM. Under a controlled setup with 100% infill density and a concentric infill pattern, the maximum ultimate tensile strength recorded was 16.95 MPa, achieved using a 90° raster angle at a printing temperature of 220 °C. In contrast, the lowest tensile strength, 14.69 MPa, was observed for samples printed at a 0° raster angle and 180 °C. The study found that increasing raster angle and temperature improved tensile strength, yield strength, and Young's modulus, attributed to enhanced interlayer bonding and increased polymer fluidity at higher temperatures.

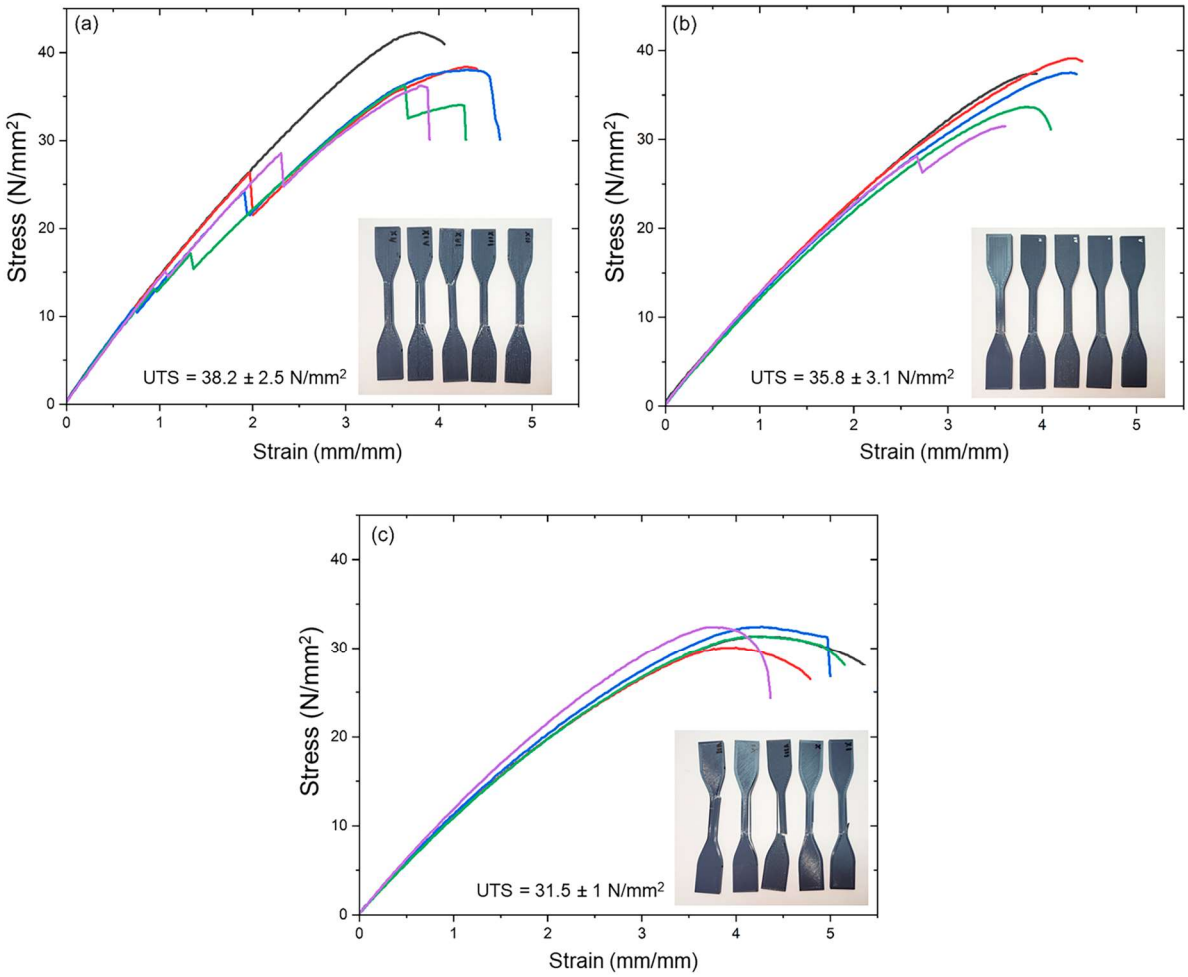

Figure 5. Stress vs. strain curves for the raster angles studied: (a) samples C1, (b) samples C2, and (c) samples C3.

Other significant work on the tensile performance of PLA was reported by Rajpurohit and Dave [53], who systematically investigated the influence of raster angle, layer height, and raster width on the tensile strength of FDM-printed PLA components. Their results demonstrated that the highest tensile strength of 47.3 MPa (higher than that of sample C1) was achieved using a 0° raster angle, a 0.1 mm layer height, and a 0.6 mm raster width. This combination optimizes inter-layer bonding and filament alignment with the loading direction [53]. This difference in tensile strength may be attributed to the fact that sample C1 has a greater layer thickness (0.2 mm).

Additionally, the observations recorded during the tensile tests revealed that the stepped behavior occurring within the elastic region of certain specimens (see Figure 5a,b) is associated with the premature failure of the outer layers, indicating that the infill structure played a predominant role in sustaining the maximum tensile load. This stepped response is most likely attributed to weak interfacial adhesion between the infill and the outer layers, particularly in the C1 specimens. On the other hand, sample C3 exhibited a fracture at a 45° angle to the load application axis, confirming that this type of raster angle tends to undergo shear deformation under load, resulting in an unfavorable redistribution of stresses and a reduction in the overall strength of the component (see Figure 5c).

A more detailed observation of the samples' fractures using a stereoscope (magnification 16×) is shown in Figure 6. Figure 6a,b shows the representative fracture of samples C1, where a fracture occurs perpendicular to the applied tensile load. Furthermore, Figure 6a revealed that the cross-section of the C1 specimens exhibited strong adhesion between the infill printing layers (z-axis), with fractures occurring primarily along the filament paths. Additionally, as observed on the left side of Figure 6a, a visible separation exists between the infill and the outer layers, indicating weak adhesion at this interface. This lack of bonding is likely the primary cause of the stepped behavior observed in Figure 5a, where the external structures (shells) fail first, followed by the infill supporting the maximum applied load (see Figure 6a). These findings are consistent with Khan et al.'s review, who highlighted inter-bead voids' formation as a recurrent defect in 3D-printed fiber-reinforced polymer composites [54]. Such voids originate from the circular geometry of the nozzle and the selected printing parameters, leading to weakened inter-bead and inter-layer bonding. Similar void morphologies were identified in the C1 samples and the outer layers of the C2 samples, suggesting that these structural discontinuities are intrinsic to the extrusion-based deposition process and contribute significantly to the observed failure modes [54].

In contrast, sample C2 showed no interlayer failures in the specimen, with fractures primarily occurring in the fibers parallel to the load direction, while the transverse fibers remain unaffected (see Figure 6c,d). Finally, a macroscopic inspection of sample C3 revealed a distinct fracture plane oriented at a 45° angle relative to the applied load (Figure 6e,f). Furthermore, delamination was characterized by the detachment of the four outermost layers from the internal fill material (see Figure 6f). This debonding was most likely caused by weak interfacial adhesion between the fill and the outer layers. This behavior observed in sample C3 highlights the tendency of fibers to undergo shear deformation under loading. This phenomenon results in an unfavorable redistribution of stresses, compromising the material's overall tensile strength. Moreover, the observed fracture behavior aligns with the results reported by Khosravani et al. [42], who confirmed through visual inspection that, in specimens with a 0° raster orientation, crack propagation occurred predominantly in the vertical direction relative to the raster layout. This indicates inter-layer failure perpendicular to the deposited filaments. In contrast, for specimens printed with raster angles of 30, 45, and 60°, the fractures followed paths aligned with

the raster direction, highlighting the critical role of raster orientation in dictating the crack trajectory and failure mechanisms in FDM-printed PLA components.

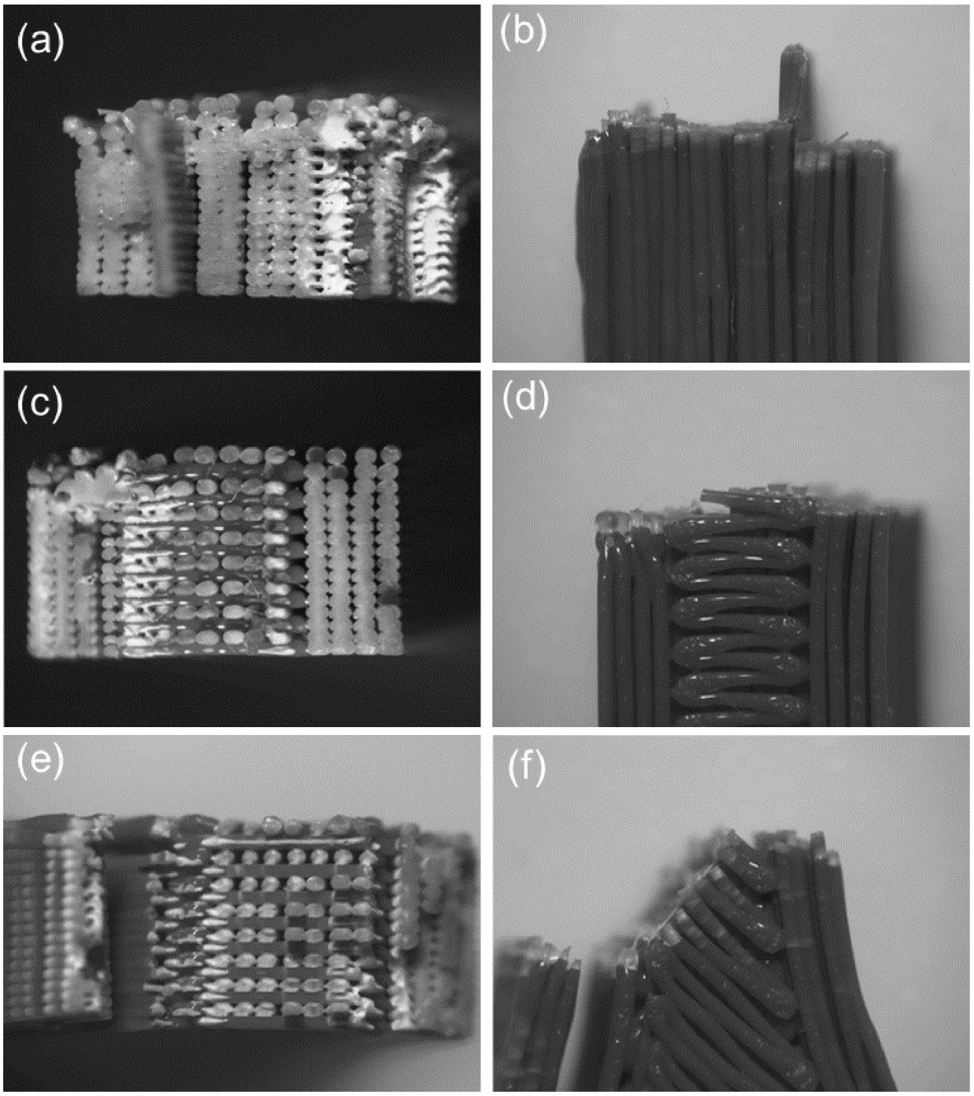

Figure 6. Stereoscopic observation of the fracture surface of the samples after the tension test: (a, b) C1, (c, d) C2, and (e, f) C3. Magnification 16×.

4. Conclusions

This study investigated the influence of raster angle on the flexural and tensile properties of 3D-printed PLA+ components. The raster angle had a significant impact on the flexural strength of the specimens. Specimens printed with a 0°/0° raster angle exhibited the highest flexural strength at 74 MPa, followed by the 0°/90° (grid) orientation at 52.1 MPa, and finally the 45°/–45° (crisscross) orientation at 40.7 MPa. This trend can be attributed to the alignment of printed filaments with the applied load. A higher number of filaments oriented perpendicular to the load direction resulted in greater flexural strength. Like flexural strength, the elastic modulus in the flexural test followed the same trend. Interestingly, the crisscross samples with the lowest flexural strength displayed a wider

plastic deformation region in the load-displacement curves than the other groups. This indicates higher ductility, implying the material's ability to absorb more energy before failure.

The tensile strength followed a similar trend to the flexural strength, with the 0°/0° raster angle orientation (C1 samples) displaying the highest value (38.2 MPa), followed by the 0°/90° orientation (C2, 35.8 MPa), and finally the 45°/–45° orientation (C3, 31.5 MPa). The majority of samples exhibited brittle behavior, characterized by minimal plastic deformation. The fracture analysis revealed several key points. C1 samples fractured predominantly at the filling section and displayed initial failure in the outer layers before the fracture was completed. Samples C3 with the 45° raster angle were fractured at an angle corresponding to the raster orientation, confirming the tendency for shear deformation and stress redistribution under load. Additionally, delamination was observed between the outer layers and the infill in C3 samples, potentially due to weak interfacial adhesion.

Overall, the results highlight the importance of selecting the raster angle to optimize the mechanical properties of 3D-printed PLA+ components. Careful consideration of the intended application and desired properties is crucial for achieving optimal component performance. This entails strategically aligning a significant proportion of fibers perpendicularly to the load in cases involving bending and parallel to the load in instances of tensile loading to enhance resistance and maximize structural integrity.

Use of AI tools declaration

The authors declare they have not used Artificial Intelligence (AI) tools in the creation of this article.

Author contributions

Andres Giovanni González: conceptualization, methodology, software, formal analysis, investigation, data curation, original draft, writing, review, editing, visualization, supervision. Juan Sebastián Ramirez and Juan Sebastián Martinez: conceptualization, methodology, validation, resources, review.

Acknowledgments

The authors are grateful to the Vice-Rector's Office of Research and Extension (VIE) of the Universidad Industrial de Santander for funding project number 4245 as part of the UIS research challenges and agendas call under the category of Applied Research or Experimental Development for 2024.

Conflict of interest

The authors declare no conflict of interest.

References

1. Oteyaka MO, Cakir FH, Sofuoglu MA (2022) Effect of infill pattern and ratio on the flexural and vibration-damping characteristics of FDM printed PLA specimens. *Mater Today Commun* 33: 104912. https://doi.org/10.1016/j.mtcomm.2022.104912
2. Rodríguez-Reyna SL, Mata C, Díaz-Aguilera JH, et al. (2023) Mechanical properties optimization for PLA, ABS and Nylon + CF manufactured by 3D FDM printing. *Mater Today Commun* 33: 104774. https://doi.org/10.1016/j.mtcomm.2022.104774
3. Adibeig MR, Vakili-Tahami F, Saeimi-Sadigh MA (2023) Numerical and experimental investigation on creep response of 3D printed polylactic acid (PLA) samples. Part I: The effect of building direction and unidirectional raster orientation. *J Mech Behav Biomed Mater* 145: 106025. https://doi.org/10.1016/j.jmbbm.2023.106025
4. Medellin-Castillo HI, Zaragoza-Siqueiros J (2019) Design and manufacturing strategies for fused deposition modelling in additive manufacturing: A review. *Chinese J Mech Eng* 32: 1–16. https://doi.org/10.1186/s10033-019-0368-0
5. Güler Ö, Tatlı O (2021) Mechanical characterization of polylactic acid polymer 3D printed materials: The effects of infill geometry. *Rev Metal* 57: e202. https://doi.org/10.3989/revmetalm.202
6. Hikmat M, Rostam S, Ahmed YM (2021) Investigation of tensile property-based Taguchi method of PLA parts fabricated by FDM 3D printing technology. *Results Eng* 11: 100264. https://doi.org/10.1016/j.rineng.2021.100264
7. El Magri A, Vaudreuil S (2021) Optimizing the mechanical properties of 3D-printed PLA graphene composite using response surface methodology. *Arch Mater Sci Eng* 112: 13–22. https://doi.org/10.5604/01.3001.0015.5928
8. Dey A, Yodo N (2019) A systematic survey of FDM process parameter optimization and their influence on part characteristics. *J Manuf Mater Process* 3: 64–94. https://doi.org/10.3390/jmmp3030064
9. Bhayana M, Singh J, Sharma A, et al. (2023) A review on optimized FDM 3D printed wood/PLA bio composite material characteristics. *Mater Today Proc.* https://doi.org/10.1016/j.matpr.2023.03.029
10. Patel R, Desai C, Kushwah S, et al. (2022) A review article on FDM process parameters in 3D printing for composite materials. *Mater Today Proc* 60: 2162–2166. https://doi.org/10.1016/j.matpr.2022.02.385
11. Wang G, Yang Y, Liu C, et al. (2023) 3D printed TPMS structural PLA/GO scaffold: Process parameter optimization, porous structure, mechanical and biological properties. *J Mech Behav Biomed Mater* 142: 105848. https://doi.org/10.1016/j.jmbbm.2023.105848
12. Benamira M, Benhassine N, Ayad A, et al. (2023) Investigation of printing parameters effects on mechanical and failure properties of 3D printed PLA. *Eng Fail Anal* 148: 107218. https://doi.org/10.1016/j.engfailanal.2023.107218
13. Lubombo C, Huneault MA (2018) Effect of infill patterns on the mechanical performance of lightweight 3D-printed cellular PLA parts. *Mater Today Commun* 17: 214–228. https://doi.org/10.1016/j.mtcomm.2018.09.017

14. Almansoori K, Pervaiz S (2023) Effect of layer height, print speed and cell geometry on mechanical properties of marble PLA based 3D printed parts. *Smart Mater Manuf* 1: 100023. https://doi.org/10.1016/j.smmf.2023.100023
15. Karimi HR, Khedri E, Nazemzadeh N, et al. (2023) Effect of layer angle and ambient temperature on the mechanical and fracture characteristics of unidirectional 3D printed PLA material. *Mater Today Commun* 35: 106174. https://doi.org/10.1016/j.mtcomm.2023.106174
16. Saravana Kumar M, Farooq MU, Ross NS, et al. (2023) Achieving effective interlayer bonding of PLA parts during the material extrusion process with enhanced mechanical properties. *Sci Rep* 13: 6800. https://doi.org/10.1038/s41598-023-33510-7
17. Camargo JC, Machado AR, Almeida EC, et al. (2019) Mechanical properties of PLA-graphene filament for FDM 3D printing. *Int J Adv Manuf Technol* 103: 2423–2443. https://doi.org/10.1007/s00170-019-03532-5
18. Karad AS, Sonawwanay PD, Naik M, et al. (2023) Experimental study of effect of infill density on tensile and flexural strength of 3D printed parts. *J Eng Appl Sci* 70: 104. https://doi.org/10.1186/s44147-023-00273-x
19. Karad AS, Sonawwanay PD, Naik M, et al. (2023) Experimental tensile strength analysis of ABS material through FDM technique. *Mater Today Proc* 103: 506–512. https://doi.org/10.1016/j.matpr.2023.09.216
20. Khan SF, Zakaria H, Chong YL, et al. (2018) Effect of infill on tensile and flexural strength of 3D printed PLA parts. *IOP Conf Ser Mater Sci Eng* 429: 012101. https://doi.org/10.1088/1757-899X/429/1/012101
21. Tanveer MQ, Mishra G, Mishra S, et al. (2022) Effect of infill pattern and infill density on mechanical behaviour of FDM 3D printed parts—A current review. *Mater Today Proc* 62: 100–108. https://doi.org/10.1016/j.matpr.2022.02.310
22. Letcher T, Waytashek M (2014) Material property testing of 3D-printed specimen in PLA on an entry-level 3D printer. ASME 2014 International Mechanical Engineering Congress and Exposition, Montreal, Quebec, Canada. https://doi.org/10.1115/IMECE2014-39379
23. Balasubramanian M, Saravanan R, Sathish T, et al. (2024) Investigating the influence of strain rate on tensile, flexural, and ILSS of fused deposition modeling printed PLA polymer. *J Mater Eng Perform*. https://doi.org/10.1007/s11665-024-10180-8
24. Gajjar T, Yang RC, Ye L, et al. (2025) Effects of key process parameters on tensile properties and interlayer bonding behavior of 3D printed PLA using fused filament fabrication. *Prog Addit Manuf* 10: 1261–1280. https://doi.org/10.1007/s40964-024-00704-y
25. Hasan A, Fahad M, Khan MA (2024) Effect of print parameters on the tensile strength and built time of FDM-printed PLA parts. *Int J Adv Manuf Technol* 132: 3047–3065. https://doi.org/10.1007/s00170-024-13506-x
26. Ambade V, Rajurkar S, Awari G, et al. (2025) Influence of FDM process parameters on tensile strength of parts printed by PLA material. *Int J Interact Des Manuf* 19: 573–584. https://doi.org/10.1007/s12008-023-01490-7
27. Gopi Mohan R, Santhosh K, Iyer RV, et al. (2021) Comparative analysis of mechanical properties of FDM printed parts based on raster angles. *Mater Today Proc* 47: 4730–4734. https://doi.org/10.1016/j.matpr.2021.05.649
28. Torres J, Cotelo J, Karl J, et al. (2015) Mechanical property optimization of FDM PLA in shear with multiple objectives. *JOM* 67: 1183–1193. https://doi.org/10.1007/s11837-015-1367-y

29. Kadhum AH, Al-Zubaidi S, Abdulkareem SS (2023) Effect of the infill patterns on the mechanical and surface characteristics of 3D printing of PLA, PLA+ and PETG materials. *ChemEngineering* 7: 46. https://doi.org/10.3390/chemengineering7030046
30. Tan MA, Yeoh CK, Teh PL, et al. (2021) Effect of infill density and raster angle on the mechanical properties of PLA. *J Phys Conf Ser* 2080: 012002. https://doi.org/10.1088/1742-6596/2080/1/012002
31. Li H, Wang T, Sun J, et al. (2018) The effect of process parameters in fused deposition modelling on bonding degree and mechanical properties. *Rapid Prototyp J* 24: 80–92. https://doi.org/10.1108/RPJ-06-2016-0090
32. Abdullah Z, Ting HY, Ali MAM, et al. (2018) The effect of layer thickness and raster angles on tensile strength and flexural strength for fused deposition modeling (FDM) parts. *J Adv Manuf Technol* 12: 147–158. https://jamt.utem.edu.my/jamt/article/view/4905
33. Dawoud M, Taha I, Ebeid SJ (2016) Mechanical behaviour of ABS: An experimental study using FDM and injection moulding techniques. *J Manuf Process* 21: 39–45. https://doi.org/10.1016/j.jmapro.2015.11.002
34. Ahn SJ, Lee H, Cho KJ (2024) 3D printing with a 3D printed digital material filament for programming functional gradients. *Nat Commun* 15: 3605. https://doi.org/10.1038/s41467-024-47480-5
35. Vega V, Clements J, Lam T, et al. (2011) The effect of layer orientation on the mechanical properties and microstructure of a polymer. *J Mater Eng Perform* 20: 978–988. https://doi.org/10.1007/s11665-010-9740-z
36. Ayatollahi MR, Nabavi-Kivi A, Bahrami B, et al. (2020) The influence of in-plane raster angle on tensile and fracture strengths of 3D-printed PLA specimens. *Eng Fract Mech* 237: 107225. https://doi.org/10.1016/j.engfracmech.2020.107225
37. Khosravani MR, Anders D, Reinicke T (2023) Effects of post-processing on the fracture behavior of surface-treated 3D-printed parts. *CIRP J Manuf Sci Technol* 46: 148–156. https://doi.org/10.1016/j.cirpj.2023.08.006
38. Albadrani MA (2023) Effects of raster angle on the elasticity of 3D-printed polylactic acid and polyethylene terephthalate glycol. *Designs* 7: 112. https://doi.org/10.3390/designs7050112
39. Singh J, Goyal KK, Kumar R (2022) Effect of filling percentage and raster style on tensile behavior of FDM produced PLA parts at different build orientation. *Mater Today Proc* 63: 433–439. https://doi.org/10.1016/j.matpr.2022.03.444
40. Khosravani MR, Berto F, Ayatollahi MR, et al. (2022) Characterization of 3D-printed PLA parts with different raster orientations and printing speeds. *Sci Rep* 12: 1016. https://doi.org/10.1038/s41598-022-05005-4
41. Srinivasan Ganesh Iyer S, Keles O (2022) Effect of raster angle on mechanical properties of 3D printed short carbon fiber reinforced acrylonitrile butadiene styrene. *Compos Commun* 32: 101163. https://doi.org/10.1016/j.coco.2022.101163
42. Sandanamsamy L, Mogan J, Rajan K, et al. (2023) Effect of process parameter on tensile properties of FDM printed PLA. *Mater Today Proc* 109: 1–6. https://doi.org/10.1016/j.matpr.2023.03.217
43. Rodríguez-Panes A, Claver J, Camacho AM (2018) The influence of manufacturing parameters on the mechanical behaviour of PLA and ABS pieces manufactured by FDM: A comparative analysis. *Mater* 11: 8. https://doi.org/10.3390/ma11081333

44. Dawood LL, AlAmeen ES (2024) Influence of infill patterns and densities on the fatigue performance and fracture behavior of 3D-printed carbon fiber-reinforced PLA composites. *AIMS Mater Sci* 11: 833–857. https://doi.org/10.3934/matersci.2024041
45. Khosravani MR, Soltani P, Reinicke T (2023) Failure and fracture in adhesively bonded 3D-printed joints: An overview on the current trends. *Eng Fail Anal* 153: 107574. https://doi.org/10.1016/j.engfailanal.2023.107574
46. Aloyaydi BA, Sivasankaran S, Ammar HR (2019) Influence of infill density on microstructure and flexural behavior of 3D printed PLA thermoplastic parts processed by fusion deposition modeling. *AIMS Mater Sci* 6: 1033–1048. https://doi.org/10.3934/matersci.2019.6.1033
47. Ferreira R, Amatte I, Dutra T, et al. (2017) Experimental characterization and micrography of 3D printed PLA and PLA reinforced with short carbon fibers. *Compos Part B Eng* 124: 88–100. https://doi.org/10.1016/j.compositesb.2017.05.013
48. ASTM International (2022) Standard test method for tensile properties of plastics. ASTM D638-22. https://doi.org/10.1520/D0638-22
49. ASTM International (2017) Standard test methods for flexural properties of unreinforced and reinforced plastics and electrical insulating materials. ASTM D790-17. https://doi.org/10.1520/D0790-17
50. Liu X, Zhang M, Li S, et al. (2017) Mechanical property parametric appraisal of fused deposition modeling parts based on the gray Taguchi method. *Int J Adv Manuf Technol* 89: 2387–2397. https://doi.org/10.1007/s00170-016-9263-3
51. Jaya Christiyan KG, Chandrasekhar U, Venkateswarlu K (2016) Flexural properties of PLA components under various test condition manufactured by 3D printer. *J Inst Eng India Ser C* 97: 277–283. https://doi.org/10.1007/s40032-016-0344-8
52. Rivera-López F, Pavón MML, Correa EC, et al. (2024) Effects of nozzle temperature on mechanical properties of polylactic acid specimens fabricated by fused deposition modeling. *Polymers* 16: 1867. https://doi.org/10.3390/polym16131867
53. Rajpurohit SR, Dave HK (2018) Effect of process parameters on tensile strength of FDM printed PLA part. *Rapid Prototyp J* 24: 1317–1324. https://doi.org/10.1108/RPJ-06-2017-0134
54. Khan T, Ali M, Riaz Z, et al. (2024) Recent developments in improving the fracture toughness of 3D-printed fiber-reinforced polymer composites. *Compos Part B Eng* 283: 111622. https://doi.org/10.1016/j.compositesb.2024.111622

AIMS Press